Acta Cryst E CRYSTALLOGRAPHIC COMMUNICATIONS

ISSN 2056-9890

Crystal structures of deuterated sodium molybdate dihydrate and sodium tungstate dihydrate from time-of-flight neutron powder diffraction

A. Dominic Fortes

ISIS Facility, Rutherford Appleton Laboratory, Harwell Science and Innovation Campus, Didcot, Oxfordshire OX11 0QX, England, Department of Earth Sciences, University College London, Gower Street, London WC1E 6BT, England, and Department of Earth and Planetary Sciences, Birkbeck, University of London, Malet Street, London WC1E 7HX, England. *Correspondence e-mail: andrew.fortes@ucl.ac.uk

Received 1 June 2015
Accepted 10 June 2015

Edited by M. Weil, Vienna University of Technology, Austria

Keywords: neutron powder diffraction; sodium molybdate dihydrate; sodium tungstate dihydrate

CCDC references: 1406122; 1406121
Supporting information: this article has supporting information at journals.iucr.org/e

Time-of-flight neutron powder diffraction data have been measured from ~90 mol% deuterated isotopologues of $Na_2MoO_4{\cdot}2H_2O$ and $Na_2WO_4{\cdot}2H_2O$ at 295 K to a resolution of sin $(\theta)/\lambda = 0.77$ Å^{-1}. The use of neutrons has allowed refinement of structural parameters with a precision that varies by a factor of two from the heaviest to the lightest atoms; this contrasts with the X-ray based refinements where precision may be > 20× poorer for O atoms in the presence of atoms such as Mo and W. The accuracy and precision of interatomic distances and angles are in excellent agreement with recent X-ray single-crystal structure refinements whilst also completing our view of the hydrogen-bond geometry to the same degree of statistical certainty. The two structures are isotypic, space-group *Pbca*, with all atoms occupying general positions, being comprised of edge- and corner-sharing NaO_5 and NaO_6 polyhedra that form layers parallel with (010) interleaved with planes of XO_4 (X = Mo, W) tetrahedra that are linked by chains of water molecules along [100] and [001]. The complete structure is identical with the previously described molybdate [Capitelli *et al.* (2006). *Asian J. Chem.* **18**, 2856–2860] but shows that the purported three-centred interaction involving one of the water molecules in the tungstate [Farrugia (2007). *Acta Cryst.* E**63**, i142] is in fact an ordinary two-centred 'linear' hydrogen bond.

1. Chemical context

Na_2MoO_4 and Na_2WO_4 are unusual amongst the alkali metal mono-molybdates and mono-tungstates in being highly soluble in water *and* forming polyhydrated crystals. Additionally, sodium apparently plays a significant role in the solvation of other alkali metal ions to form a range of double molybdate and tungstate hydrates (Klevtsova *et al.*, 1990; Klevtsov *et al.*, 1997; Mirzoev *et al.*, 2010), for example, $Na_3K(MoO_4)_2{\cdot}9H_2O$. Both dihydrate and decahydrate varieties of the two title compounds are known, their solubilities as a function of temperature being well characterised (Funk, 1900; Zhilova *et al.*, 2008). The structures of the decahydrates have not yet been reported, although I have established that they are not isotypic with the sodium sulfate analogue, $Na_2SO_4{\cdot}10H_2O$, as had hitherto been thought.

The dihydrates have been the subject of extensive crystallographic studies, from descriptions of their density, habit and measurements of interfacial angles (Svanberg & Struve, 1848; Zenker, 1853; Rammelsberg, 1855; Marignac, 1863; Delafontaine, 1865; Ullik, 1867; Clarke, 1877; Zambonini, 1923), through to determination of absolute unit-cell parameters (Pistorius & Sharp, 1961), and subsequent solution and

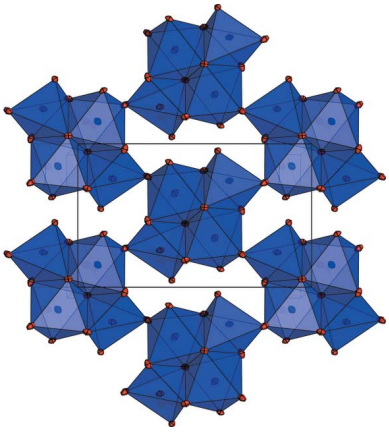

Table 1
Comparison of the X—O (X = Mo, W) and Na—O bond lengths (Å) in $Na_2MoO_4{\cdot}2D_2O$ and $Na_2WO_4{\cdot}2D_2O$ with those of the protonated isotopologues reported in the literature.

	$Na_2MoO_4{\cdot}2D_2O$	$Na_2MoO_4{\cdot}2H_2O$	$Na_2WO_4{\cdot}2D_2O$	$Na_2WO_4{\cdot}2H_2O$
	This work	Capitelli *et al.* (2006)	This work	Farrugia (2007)
X—O1	1.773 (2)	1.772 (1)	1.785 (2)	1.776 (3)
X—O2	1.764 (1)	1.767 (1)	1.778 (2)	1.778 (3)
X—O3	1.750 (2)	1.751 (1)	1.766 (2)	1.761 (3)
X—O4	1.776 (2)	1.778 (1)	1.783 (2)	1.787 (3)
Mean X—O	1.766	1.767	1.778	1.776
Na1—O2	2.437 (3)	2.446 (2)	2.433 (2)	2.442 (3)
Na1—O2$^{(i)}$	2.417 (3)	2.419 (2)	2.412 (3)	2.416 (3)
Na1—O3$^{(ii)}$	2.482 (3)	2.481 (2)	2.479 (3)	2.480 (3)
Na1—O4$^{(iii)}$	2.410 (3)	2.395 (2)	2.399 (2)	2.388 (3)
Na1—O5	2.476 (3)	2.456 (2)	2.479 (3)	2.464 (4)
Na1—O6	2.426 (3)	2.423 (2)	2.443 (3)	2.433 (3)
Mean Na1—O	2.441	2.437	2.441	2.437
Na2—O1^{iv}	2.312 (3)	2.319 (2)	2.320 (2)	2.323 (3)
Na2—O2	2.363 (3)	2.354 (2)	2.355 (2)	2.346 (3)
Na2—O3^{v}	2.339 (3)	2.341 (2)	2.328 (2)	2.331 (3)
Na2—O5	2.415 (3)	2.403 (2)	2.409 (3)	2.396 (3)
Na2—O6^{vi}	2.305 (3)	2.300 (2)	2.311 (2)	2.304 (3)
Mean Na2—O	2.347	2.343	2.345	2.340

Symmetry codes: (i) $1-x, 1-y, 1-z$; (ii) $-\frac{1}{2}+x, \frac{3}{2}-y, 1-z$; (iii) $\frac{1}{2}-x, -\frac{1}{2}+y, z$; (iv) $\frac{1}{2}+x, \frac{3}{2}-y, 1-z$; (v) $\frac{3}{2}-x, -\frac{1}{2}+y, z$; (vi) $\frac{1}{2}+x, y, \frac{3}{2}-z$.

refinement of their structures (Mitra & Verma, 1969; Okada *et al.*, 1974; Matsumoto *et al.*, 1975; Atovmyan & D'yachenko, 1969; Capitelli *et al.*, 2006; Farrugia, 2007). However, the presence of heavy atoms in these materials makes it impossible to achieve a uniform precision on all structural parameters using X-rays, and even with single-crystal methods that purport to identify hydrogen positions there may be significant inaccuracies. Such problems are minimised using a neutron radiation probe since the coherent neutron scattering lengths of the constituent elements differ by less than a factor of two, being 6.715 fm for Mo, 4.86 fm for W, 3.63 fm for Na, 5.803 fm for O, and 6.67 fm for ^{2}D (Sears, 1992). Thus one can locate accurately all of the light atoms and obtain a uniform level of precision on their coordinates and displacement parameters. Since the incoherent neutron scattering cross section of ^{1}H is large (80.3 barns) it is usual to prepare perdeuterated specimens whenever possible (the incoherent cross section of ^{2}D being only 2.1 barns) as this optimises the coherent Bragg scattering signal above the background, reducing the counting times required for a high-precision structure refinement from many days to a matter of hours on the instrument used for these measurements. These data were therefore measured using $Na_2MoO_4{\cdot}2D_2O$ and $Na_2WO_4{\cdot}2D_2O$ samples.

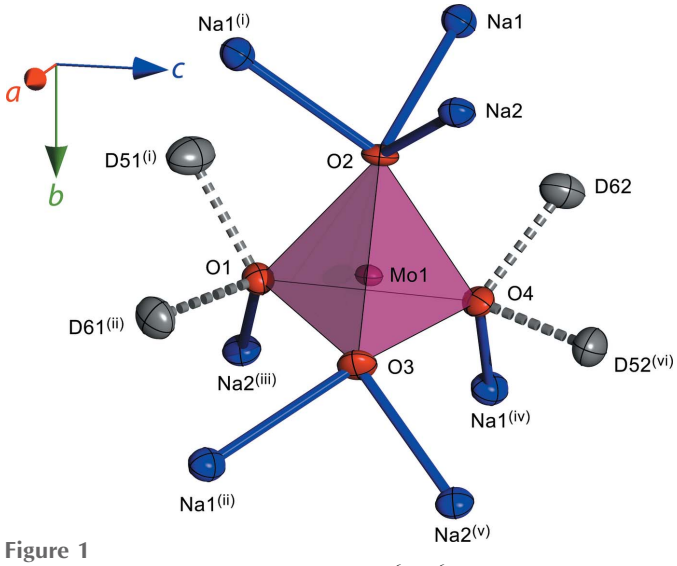

Figure 1
First and second coordination shell of Mo^{6+}/W^{6+} in the title compounds, revealing differences in the environment of each apical O^{2-} that are responsible for the variations in Mo–O and W–O bond lengths. Anisotropic displacement ellipsoids are drawn at the 50% probability level. [Symmetry codes: (i) $1-x, 1-y, 1-z$; (ii) $\frac{1}{2}+x, \frac{3}{2}-y, 1-z$; (iii) $-\frac{1}{2}+x, \frac{3}{2}-y, 1-z$; (iv) $\frac{1}{2}-x, \frac{1}{2}+y, z$; (v) $\frac{3}{2}-x, \frac{1}{2}+y, z$; (vi) $1-x, \frac{1}{2}+y, 1.5-z$.]

The occurrence of polyhydrated forms of both Na_2MoO_4 and Na_2WO_4 suggests that both would be excellent candidates for the formation of hydrogen-bonded complexes with water-soluble organics, such as amino acids, producing metal-organic crystals with potentially useful optical properties (*cf.*, glycine lithium molybdate; Fleck *et al.*, 2006). High-pressure polymorphs of $Na_2MoO_4{\cdot}2H_2O$ and $Na_2WO_4{\cdot}2H_2O$ are indicated from Raman scattering studies (Luz-Lima *et al.*, 2010; Saraiva *et al.*, 2013). Characterising the structures and properties of the title compounds provides an essential foundation on which to build future studies of the high-pressure phases, of the as-yet incomplete decahydrate structures and any related organic-bearing hydrates.

2. Structural commentary

$Na_2MoO_4{\cdot}2H_2O$ and $Na_2WO_4{\cdot}2H_2O$ are isotypic, crystallizing in the orthorhombic space group *Pbca*; all atoms occupy

Table 2
Comparison of the water molecule and hydrogen bond geometry (Å, °) in $Na_2MoO_4{\cdot}2D_2O$ and $Na_2WO_4{\cdot}2D_2O$ with the protonated isotopologues as reported in the literature. Note the inclusion of the contact O5–D51···O3, which forms the longer 'branch' of Farrugia's proposed bifurcated hydrogen bond.

	$Na_2MoO_4{\cdot}2D_2O$	$Na_2MoO_4{\cdot}2H_2O$	$Na_2WO_4{\cdot}2D_2O$	$Na_2WO_4{\cdot}2H_2O$
	This work	Capitelli *et al.* (2006)	This work	Farrugia (2007)
O5—D51	0.977 (2)	0.68 (3)	0.970 (2)	0.86 (3)
O5—D52	0.966 (2)	0.76 (3)	0.959 (2)	0.86 (3)
D51—O5—D52	106.0 (2)	98 (4)	106.0 (2)	100 (5)
D51···O1$^{(i)}$	1.874 (2)	2.16 (3)	1.873 (2)	2.09 (4)
O5—D51···O1$^{(i)}$	167.9 (2)	167 (4)	168.2 (2)	145 (6)
D51···O3$^{(ii)}$	–	–	–	2.70 (6)
O5—D51···O3$^{(ii)}$	–	–	–	122 (5)
D52···O4$^{(ii)}$	1.846 (3)	2.07 (3)	1.863 (2)	1.98 (3)
O5—D52···O4$^{(ii)}$	171.2 (2)	176 (3)	170.9 (2)	174 (6)
O6—D61	0.972 (2)	0.83 (3)	0.968 (2)	0.86 (3)
O6—D62	0.972 (2)	0.71 (3)	0.966 (2)	0.86 (3)
D61—O6—D62	103.0 (2)	105 (3)	103.2 (2)	95 (5)
D61···O1	1.816 (2)	2.01 (3)	1.834 (2)	1.95 (3)
O6—D61···O1	167.0 (2)	167 (3)	167.0 (2)	167 (6)
D62···O4$^{(iii)}$	1.868 (4)	2.08 (3)	1.876 (2)	2.02 (4)
O6—D62···O4$^{(iii)}$	168.7 (2)	170 (3)	168.7 (2)	159 (6)

Symmetry codes: (i) $1-x, 1-y, 1-z$; (ii) $1-x, -\frac{1}{2}+y, \frac{3}{2}-z$; (iii) $-\frac{1}{2}+x, \frac{3}{2}-y, 1-z$.

general positions (Wyckoff sites 8*c*). Note that the atom labelling scheme and space-group setting used here follows Farrugia (2007); consequently there are some differences with respect to other literature sources, although equivalent contacts are referred to in Table 1 and Table 2. The X^{6+} ions (X = Mo, W) are tetrahedrally coordinated by O^{2-}, the Mo—O and W—O bond lengths varying slightly according to the type of coordination adopted by a particular apex: O1 and O4 are each coordinated to Na^+ and each also accepts two hydrogen bonds; O2 is coordinated to three Na^+ ions and O3 is coordinated to two Na^+ ions (Fig. 1). In both title compounds, X–O1 and X–O4 are the longest contacts and X–O3 is the shortest contact in the tetrahedral oxyanion. The mean Mo—O and W—O bond lengths are in good agreement with those found in the anhydrous crystals (Fortes, 2015). Furthermore, each of the absolute Mo—O bond lengths are identical (within error) to those found by Capitelli *et al.* (2006); the agreement in W—O bond lengths with Farrugia (2007) is marginally poorer.

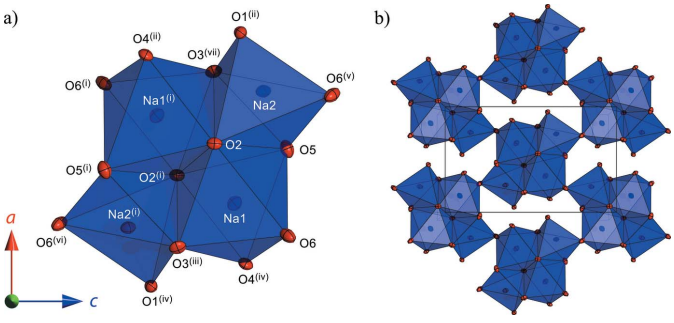

Figure 2
(*a*) Arrangement of NaO_x polyhedra into edge-sharing clusters comprised of two $Na1O_6$ octahedra and two $Na2O_5$ square pyramids; (*b*) Arrangement of the clusters shown in (*a*) by corner sharing to form 'slabs' parallel (010). Ellipsoids are drawn at the 50% probability level. [Symmetry codes: (i) $1-x, 1-y, 1-z$; (ii) $\frac{1}{2}+x, \frac{3}{2}-y, 1-z$; (iii) $-\frac{1}{2}+x, \frac{3}{2}-y, 1-z$; (iv) $\frac{1}{2}-x, -\frac{1}{2}+y, z$; (v) $\frac{1}{2}+x, y, \frac{3}{2}-z$; (vi) $\frac{1}{2}-x, 1-y, \frac{1}{2}+z$; (vii) $\frac{3}{2}-x, -\frac{1}{2}+y, z$.]

The Na^+ ions occupy two inequivalent sites: in one, Na^+ is six-fold coordinated by two water molecules and four XO_4^{2-} oxygen atoms, yielding an octahedral arrangement; in the second, Na^+ is five-fold coordinated by two water molecules and three XO_4^{2-} oxygen atoms, yielding a square-pyramidal arrangement. These two polyhedra share a common edge (O2–O5) and are connected, moreover, with their inversion-centre-related neighbours along three other shared edges to form a cluster (Fig. 2*a*). The clusters corner-share *via* O6 to create a 'slab' parallel to (010) (Fig. 2*b*). The mean Na—O bond lengths are statistically identical in $Na_2MoO_4{\cdot}2D_2O$ and $Na_2WO_4{\cdot}2D_2O$ being ∼1.6% longer in the NaO_6 octahedra and ∼2.3% shorter in the NaO_5 polyhedra than Na—O bonds in the anhydrous crystals (Fortes, 2015). The agreement in Na—O bond lengths with the X-ray single crystal studies of Capitelli *et al.* (2006) and Farrugia (2007) is very good. Overall, the agreement in bond lengths and angles for the two independently refined data sets is excellent (Tables 1 and 2).

Although it is more usual to find Na^+ in octahedral coordination, there are abundant examples of Na^+ in five-fold coordination, including instances where the NaO_5 polyhedron adopts a square-pyramidal arrangement (Beurskens & Jeffrey, 1961; Císařová; *et al.*, 2001; Sharma *et al.*, 2005; Smith & Wermuth, 2014; Aksenov *et al.*, 2014) or the alternative trigonal-bipyramidal arrangement (Mereiter, 2013; Smith, 2013). A similar combination of NaO_6 and NaO_5 polyhedra to that found in the title compounds occurs in the closely-related hydrates $Na_2CrO_4{\cdot}1.5H_2O$ and $Na_2SeO_4{\cdot}1.5H_2O$ (Kahlenberg, 2012; Weil & Bonneau, 2014). The two water molecules form hydrogen-bonded chains between the O1 and O4 atoms of the tetrahedral oxyanions; O5-related chains extend along [001] and O6-related chains crosslink them in a staggered fashion

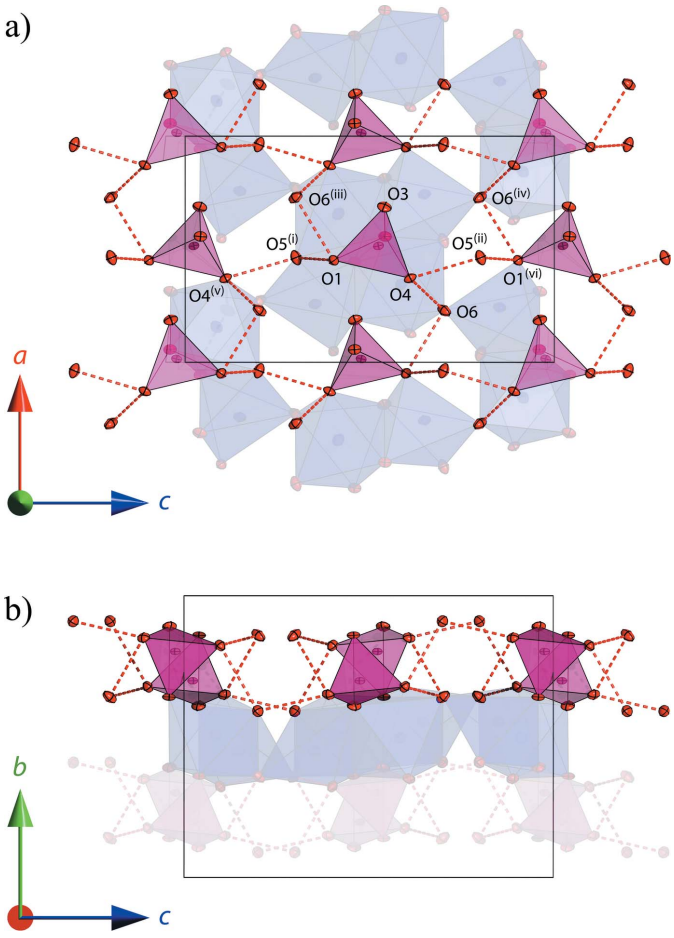

Figure 3
(*a*) View down the *b* axis of the network of water-linked tetrahedral oxyanions; chains linked by O5 extend along [001] whereas crosslinkages through O6 are staggered along [100]. (*b*) View of the same structure along the *c* axis. Ellipsoids are drawn at the 50% probability level. [Symmetry codes: (i) $1-x, 1-y, 1-z$; (ii) $1-x, \frac{1}{2}+y, \frac{3}{2}-z$; (iii) $\frac{1}{2}+x, \frac{3}{2}-y, 1-z$; (iv) $\frac{1}{2}+x, y, \frac{3}{2}-z$; (v) $x, \frac{3}{2}-y, -\frac{1}{2}+z$; (vi) $x, \frac{3}{2}-y, \frac{1}{2}+z$.]

along [100]. Fig. 3(*a*) and 3(*b*) depict the spatial relationship between this 'net' of water linked tetrahedra and the adjacent 'slab' of corner-linked Na—O polyhedral clusters. The layers shown in Fig. 3(*b*) alternate to create the three-dimensional structure and are no doubt responsible for the macro-scale platy habit of the crystals.

There are no significant differences in the hydrogen bond geometries of the molybdate or tungstate crystals. The most recent X-ray single-crystal diffraction study of $Na_2WO_4{\cdot}2H_2O$ (Farrugia, 2007) implied that one of the water molecules (O5) was involved in a weaker three-centred interaction, although a similarly recent measurement of $Na_2MoO_4{\cdot}2H_2O$ (Capitelli *et al.*, 2006) identified a 'normal' linear two-centred interaction for this bond. This work, using neutrons, has been able to accurately and precisely characterise the hydrogen bond geometry, showing that the latter is true for both structures; there is no bifurcated bond and all hydrogen-bonded interactions are of the linear two-centred variety. Presumably the error in Farrugia's analysis arose due to the substantial absorption correction required (μ = 18.7 mm^{-1}) for an accurate structure refinement from X-ray single-crystal data.

Raman spectra of $Na_2MoO_4{\cdot}2H_2O$ and $Na_2MoO_4{\cdot}2D_2O$ were first reported by Mahadevan Pillai *et al.* (1997); subsequently, Luz-Lima *et al.* (2010) and Saraiva *et al.* (2013) published the Raman spectra of $Na_2MoO_4{\cdot}2H_2O$ and $Na_2WO_4{\cdot}2H_2O$ as a function of temperature (13–300 K) and as a function of hydrostatic pressure (to 5 GPa). Both compounds exhibit evidence of a 'conformational change' on cooling through 120 K: the molybdate appears to undergo two high-pressure phase transitions, one at 3 GPa and the second at 4 GPa; the tungstate apparently undergoes a high-pressure phase transition at 3.9 GPa. The Raman spectra reported here (Figs. 4 and 5 and *Supporting information*) agree well with data in the literature (Table 3). The large blue-shifts in the internal vibrational frequencies of the deuterated water molecule are similar to the square root of the D:H mass ratio; the small blue-shifts of most of the internal modes of the tetrahedral oxyanions are consistent with stronger hydrogen bonding in the deuterated species, as expected (*cf.* Scheiner & Čuma, 1996; Soper & Benmore, 2008).

3. Synthesis and crystallization

Coarse polycrystalline powders of $Na_2MoO_4{\cdot}2H_2O$ (Sigma–Aldrich M1003 > 99.5%) and $Na_2WO_4{\cdot}2H_2O$ (Sigma–Aldrich 14304 > 99%) were dehydrated by drying at 673 K in air. The resulting anhydrous materials were characterised by Raman spectroscopy, X-ray and neutron powder diffraction (Fortes, 2015). This material was dissolved in D_2O (Aldrich 151882,

Table 3
Comparison of the internal vibrational mode frequencies (cm^{-1}) in fully protonated and 90 mol % deuterated isotopologues of $Na_2MoO_4{\cdot}2H_2O$ and $Na_2WO_4{\cdot}2H_2O$ with literature data.

	$Na_2MoO_4{\cdot}2H_2O$			$Na_2WO_4{\cdot}2H_2O$		
	This work (^{1}H)	This work (^{2}D)	Busey & Keller (1964)	This work (^{1}H)	This work (^{2}D)	Busey & Keller (1964)
ν_2 (XO_4^{2-})	279	271	285	276	269	276
	319	315	325	324	321	325
	335	331		330	331	
ν_4 (XO_4^{2-})	359	358		358	355	
ν_3 (XO_4^{2-})	804	801	805	804	802	808
	833	826	836	836	831	838
	842	840	843		840	
ν_1 (XO_4^{2-})				891	889	893
	894	894	897	929	928	931

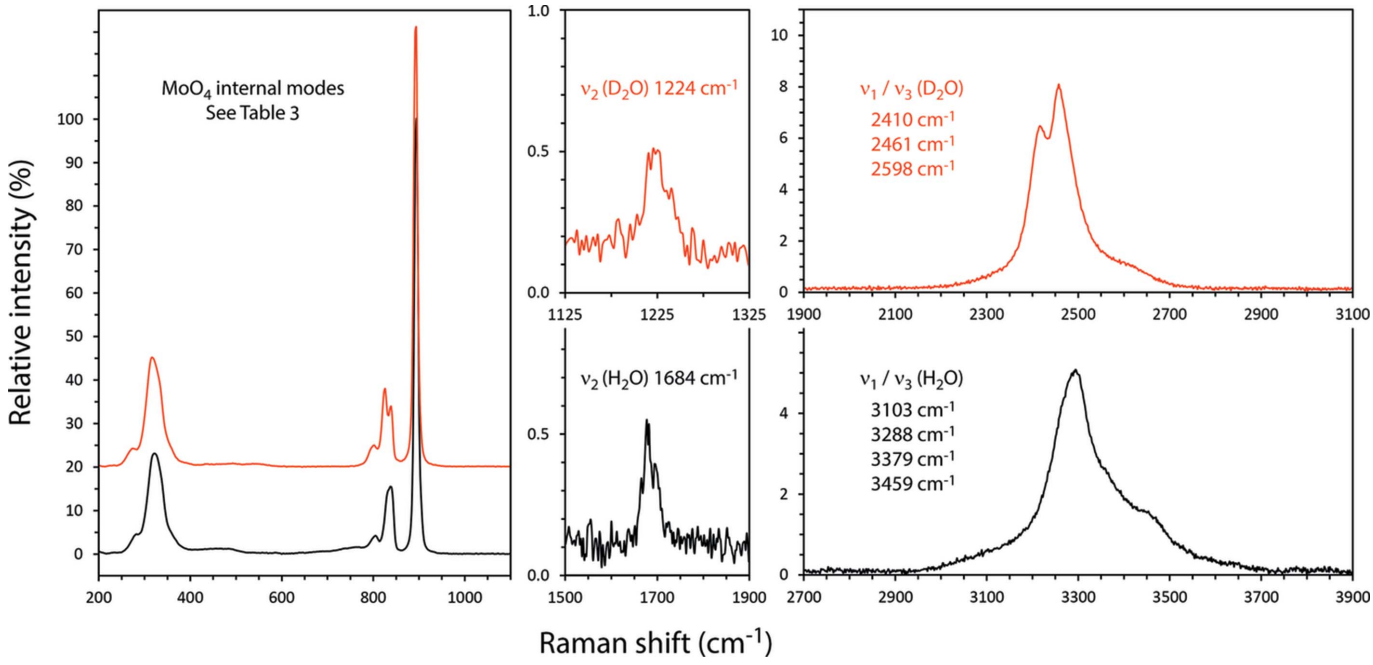

Figure 4
Raman spectra of $Na_2MoO_4{\cdot}2H_2O$ and $Na_2MoO_4{\cdot}2D_2O$ in the range 200–3900 cm^{-1}. Band positions and vibrational assignments are indicated (see also Table 3). Vertical scales show intensities relative to ν_1 (XO_4^{2-}).

99.9 atom% D) and twice recrystallized by gentle evaporation at 323 K. The molybdate crystallised with a coarse platy habit whereas the tungstate was deposited as a finer-grained material. Once the supernatant liquid was decanted, the residue was air dried on filter paper and then ground to a fine powder with an agate pestle and mortar. The powders were loaded into standard vanadium sample-holder tubes of internal diameter 11 mm to a depth not less than 20 mm (this being the vertical neutron beam dimension at the sample position). Accurate volumes and masses were determined after the diffraction measurements were complete and used to correct the data for self-shielding. The level of deuteration was determined by Raman spectroscopy (see below) to be ∼91% for both compounds.

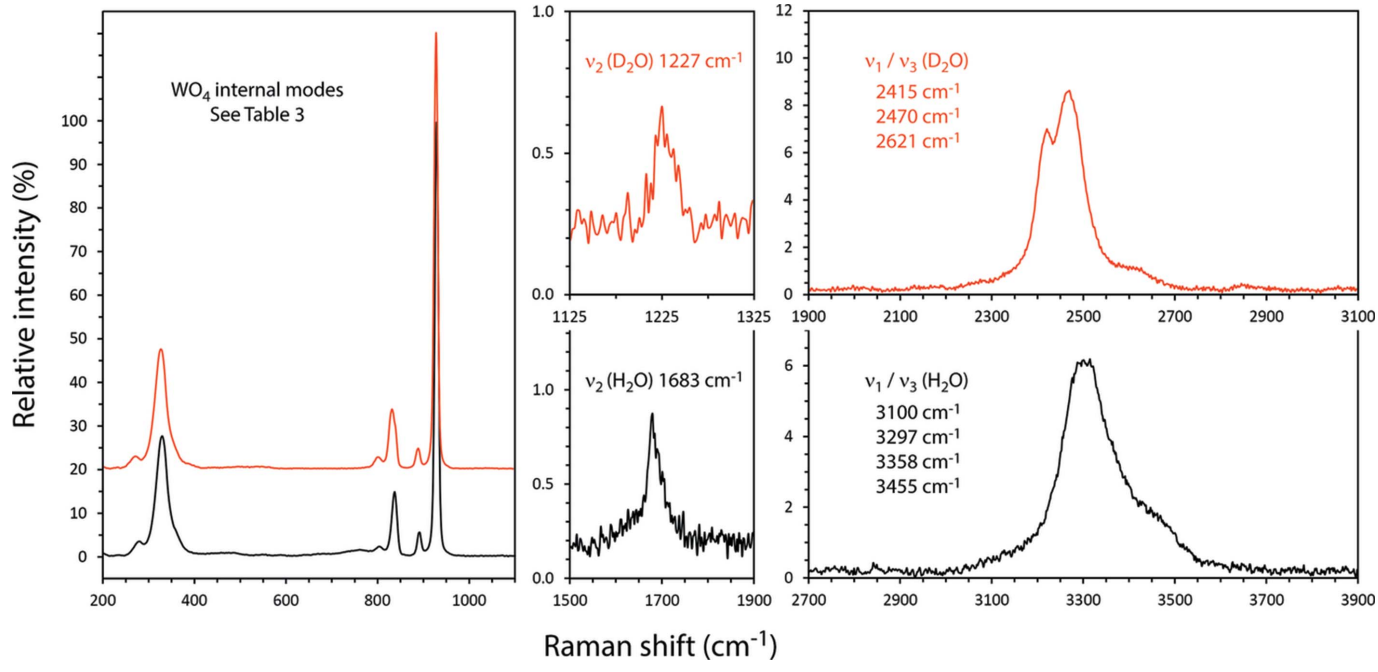

Figure 5
Raman spectra of $Na_2WO_4{\cdot}2H_2O$ and $Na_2WO_4{\cdot}2D_2O$ in the range 200–3900 cm^{-1}. Band positions and vibrational assignments are indicated (see also Table 3). Vertical scales show intensities relative to ν_1 (XO_4^{2-}).

Table 4
Experimental details.

	$Na_2MoO_4{\cdot}2D_2O$	$Na_2WO_4{\cdot}2D_2O$
Crystal data		
Chemical formula	$Na_2MoO_4{\cdot}2D_2O$	$Na_2WO_4{\cdot}2D_2O$
M_r	245.99	333.87
Crystal system, space group	Orthorhombic, *Pbca*	Orthorhombic, *Pbca*
Temperature (K)	295	295
a, b, c (Å)	8.482961 (14), 10.566170 (17), 13.83195 (3)	8.482514 (15), 10.595156 (19), 13.85640 (3)
V (Å^3)	1239.79 (1)	1245.32 (1)
Z	8	8
Radiation type	Neutron	Neutron
μ (mm^{-1})	0.03 + 0.0007 * λ	0.03 + 0.0033 * λ
Specimen shape, size (mm)	Cylinder, 38 × 11	Cylinder, 50 × 11
Data collection		
Diffractometer	HRPD, High resolution neutron powder	HRPD, High resolution neutron powder
Specimen mounting	Vanadium tube	Vanadium tube
Data collection mode	Transmission	Transmission
Scan method	Time of flight	Time of flight
Absorption correction	Analytical [data were corrected for self shielding using σ_{scatt} = 93.812 barns and $\sigma_{ab}(\lambda)$ = 3.657 barns at 1.798 Å during the normalization procedure. The linear absorption coefficient is wavelength dependent and is calculated as: μ = 0.0308 + 0.0007 * λ (mm^{-1})]	analytical [data were corrected for self shielding using σ_{scatt} = 94.190 barns and $\sigma_{ab}(\lambda)$ = 19.484 barns at 1.798 Å during the normalization procedure. The linear absorption coefficient is wavelength dependent and is calculated as: μ = 0.0284 + 0.0033 * λ (mm^{-1})]
T_{min}, T_{max}	0.685, 0.706	0.700, 0.603
2θ values (°)	$2\theta_{fixed}$ = 168.329	$2\theta_{fixed}$ = 168.329
Distance from source to specimen (mm)	95000	95000
Distance from specimen to detector (mm)	965	965
Refinement		
R factors and goodness of fit	R_p = 0.013, R_{wp} = 0.013, R_{exp} = 0.007, $R(F^2)$ = 0.05255, χ^2 = 3.534	R_p = 0.014, R_{wp} = 0.013, R_{exp} = 0.007, $R(F^2)$ = 0.04597, χ^2 = 3.312
No. of data points	4610	4610
No. of parameters	133	133

Computer programs: HRPD control software, *GSAS*/Expgui (Larsen & Von Dreele, 2000: Toby, 2001), Mantid (Arnold *et al.*, 2014: Mantid, 2013), *DIAMOND* (Putz & Brandenburg, 2006) and *publCIF* (Westrip, 2010).

Raman spectra were acquired with a B&WTek *i*-Raman plus portable spectrometer; this device uses a 532 nm laser (37 mW power at the fiber-optic probe tip) to stimulate Raman scattering, which is measured in the range 170–4000 cm^{-1} with a spectral resolution of 3 cm^{-1}. Data were collected for 600 sec at 17 mW for $Na_2MoO_4{\cdot}2H_2O$ (as

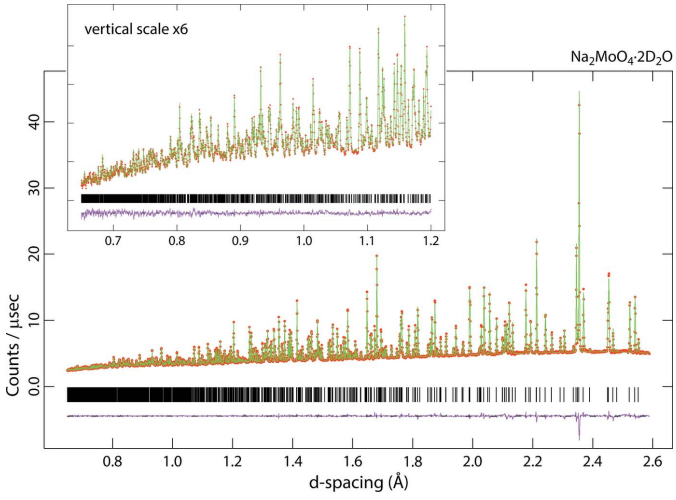

Figure 6
Neutron powder diffraction data for $Na_2MoO_4{\cdot}2D_2O$; red points are the observations, the green line is the calculated profile and the pink line beneath the diffraction pattern represents Obs−Calc. Vertical black tick marks report the expected positions of the Bragg peaks. The inset shows the data measured at short flight times (*i.e.* small *d*-spacings).

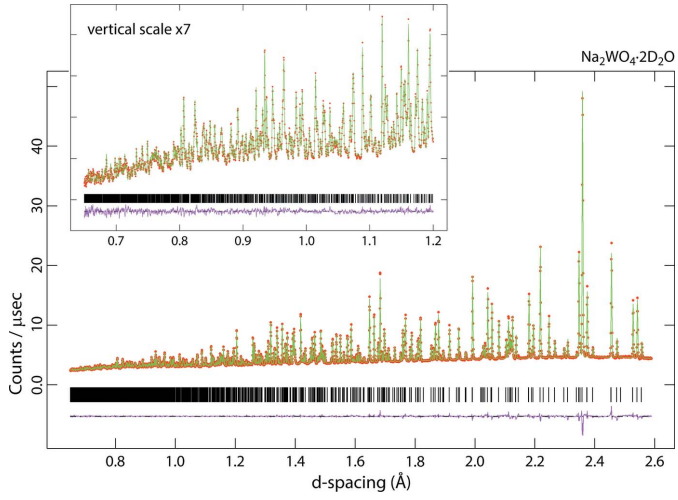

Figure 7
Neutron powder diffraction data for $Na_2WO_4{\cdot}2D_2O$; red points are the observations, the green line is the calculated profile and the pink line beneath the diffraction pattern represents Obs−Calc. Vertical black tick marks report the expected positions of the Bragg peaks. The inset shows the data measured at short flight times (*i.e.* small *d*-spacings).

bought), 180 sec at 37 mW for $Na_2MoO_4{\cdot}2D_2O$, 300 sec at 17 mW for $Na_2WO_4{\cdot}2H_2O$ (as bought) and 220 sec at 37 mW for $Na_2WO_4{\cdot}2D_2O$; after summation, the background was removed and peaks fitted using Pseudo-Voigt functions in OriginPro (OriginLab, Northampton MA). These data are provided as an electronic supplement in the form of an ASCII file. Small quantities of ordinary hydrogen were found to be present in both specimens, the proportion being determined by the ratio of the areas under the ν_1/ν_3 (H_2O) bands after normalisation relative to the height of the strong ν_1 (XO_4^{2-}) band. The molar abundance of ^1H was used to correct the diffraction data for absorption (see below) and to ensure accurate refinement of the structure (see *Refinement*).

Time-of-flight neutron diffraction patterns were collected at 295 K using the High Resolution Powder Diffractometer, HRPD (Ibberson, 2009), at the ISIS spallation neutron source, Harwell Campus, Oxfordshire, UK. Data were acquired in the range of neutron flight times from 30–130 msec (equivalent to neutron wavelengths of 1.24–5.36 Å) for 15.17 hr from the molybdate and 14.40 hr from the tungstate, equivalent to 615 and 590 μAhr of integrated proton beam current, respectively. These data sets were normalized to the incident spectrum and corrected for detector efficiency by reference to a V:Nb null-scattering standard and then subsequently corrected for the sample-specific and wavelength-dependent self-shielding using Mantid (Arnold *et al.*, 2014: Mantid, 2013). In the case of the molybdate, the number density of the specimen was determined to be 3.28 mol nm^{-3}, with a scattering cross section, allowing for the water being 9.1 mol % ^1H, σ_{scatt} = 93.81 b and an absorption cross section, σ_{abs} = 3.66 b; for the tungstate, the number density was 3.01 mol nm^{-3}, the scattering cross section, allowing for the water being 8.6 mol % ^1H, σ_{scatt} = 94.19 b and σ_{abs} = 19.48 b. Diffraction data were exported in GSAS format and analysed with the GSAS/Expgui Rietveld package (Larsen & Von Dreele, 2000: Toby, 2001). The fitted diffraction data are shown in Figs. 6 and 7.

4. Refinement

Profile refinements were done using GSAS/Expgui (Larsen & Von Dreele, 2000; Toby, 2001) starting from the coordinates reported by Farrugia (2007). Statistically significant anisotropic displacement parameters were refined for all atoms. An assumption was made that ^1H was uniformly distributed on all ^2D sites, so the neutron scattering length of ^2D was edited in GSAS in accordance with the concentration of ^1H determined by Raman spectroscopy; for the molybdate a value of 5.776 fm was used, and for the tungstate a value of 5.724 fm was adopted. Crystal data, data collection and structure refinement details are summarized in Table 4.

Acknowledgements

The author thanks the STFC ISIS facility for beam-time access and acknowledges financial support from STFC (grant No. ST/K000934/1).

References

Aksenov, S. M., Rastsvetaeva, R. K., Chukanov, N. V. & Kolitsch, U. (2014). *Acta Cryst.* B**70**, 768–775.
Arnold, O., *et al.* (2014). *Nucl. Instrum. Methods Phys. Res.* A**764**, 156–166.
Atovmyan, L. O. & D'yachenko, O. A. (1969). *J. Struct. Chem.* **10**, 416–418.
Beurskens, G. & Jeffrey, G. A. (1961). *J. Chem. Phys.* **41**, 924–929.
Busey, R. H. & Keller, O. L. (1964). *J. Chem. Phys.* **41**, 215–225.
Capitelli, F., Selim, M. & Mukherjea, K. K. (2006). *Asian J. Chem.* **18**, 2856–2860.
Císařová, I., Skála, R., Ondruš, P. & Drábek, M. (2001). *Acta Cryst.* E**57**, i32–i34.
Clarke, F. W. (1877). *Am. J. Sci. Ser. III*, **14**, 280–286.
Delafontaine, M. (1865). *J. Prakt. Chem.* **95**, 136–145.
Farrugia, L. J. (2007). *Acta Cryst.* E**63**, i142.
Fleck, M., Schwendtner, K. & Hensler, A. (2006). *Acta Cryst.* C**62**, m122–m125.
Fortes, A. D. (2015). *Acta Cryst.* E**71**, 592–596.
Funk, R. (1900). *Ber. Dtsch Chem. Ges.* **33**, 3696–3703.
Ibberson, R. M. (2009). *Nucl. Instrum. Methods Phys. Res. A*, **600**, 47–49.
Kahlenberg, V. (2012). *Z. Kristallogr.* **227**, 621–628.
Klevtsova, R. F., Glinskaya, L. A., Perepelitsa, A. P., Ishchenko, V. N. & Klevtsov, P. V. (1990). *Sov. Phys. Crystallogr.* **35**, 643–646.
Klevtsov, P. V., Glinskaya, L. A., Klevtsova, R. F. & Aleksandrov, K. S. (1997). *J. Struct. Chem.* **38**, 615–619.
Larsen, A. C. & Von Dreele, R. B. (2000). General Structure Analysis System (*GSAS*). Los Alamos National Laboratory Report LAUR 86-748, Los Alamos, New Mexico. http://www.ncnr.NIST.gov/Xtal/software/GSAS.html.
Luz-Lima, C., Saraiva, G. D., Souza Filho, A. G., Paraguassu, W., Freirea, P. T. C. & Mendes Filhoa, J. (2010). *J. Raman Spectrosc.* **41**, 576–581.
Mahadevan Pillai, V. P., Pradeep, T., Bushiri, M. J., Jayasree, R. S. & Nayar, V. U. (1997). *Spectrochim. Acta* A**53**, 867–876.
Mantid (2013). Manipulation and Analysis Toolkit for Instrument Data.; Mantid Project. http://dx.doi.org/10.5286/SOFTWARE/MANTID.
Marignac, J. C. (1863). *Ann. Chim. Phys. 3eme Ser.* **69**, 5–86.
Matsumoto, K., Kobayashi, A. & Sasaki, Y. (1975). *Bull. Chem. Soc. Jpn*, **48**, 1009–1013.
Mereiter, K. (2013). *Acta Cryst.* E**69**, i77–i78.
Mirzoev, R. S., Shetov, R. A., Ligidov, M. Kh. & El'mesova, R. M. (2010). *Russ. J. Inorg. Chem.* **55**, 96–102.
Mitra, R. P. & Verma, H. K. L. (1969). *Indian J. Chem.* **7**, 598–602.
Okada, K., Morikawa, H., Marumo, F. & Iwai, S. I. (1974). *Bull. Tokyo Inst. Technol.* **120**, 7–11.
Pistorius, C. W. F. T. & Sharp, W. E. (1961). *Acta Cryst.* **14**, 316–317.
Putz, H. & Brandenburg, K. (2006). *DIAMOND*. Crystal Impact, Bonn, Germany.
Rammelsberg, K. F. A. (1855). In *Handbuch der Krystallographischen Chemie*. Berlin: P. Jeanrenaud.
Saraiva, G. D., Luz-Lima, C., Freire, P. T. C., Ramiro de Castro, A. J., de Sousa, G. P., Melo, F. E. A., Silva, J. H. & Mendes Filho, J. (2013). *J. Mol. Struct.* **1033**, 154–161.
Scheiner, S. & Čuma, C. (1996). *J. Am. Chem. Soc.* **118**, 1511–1521.
Sears, V. F. (1992). *Neutron News*, **3**, 26–37.
Sharma, R. P., Bala, R., Sharma, R. & Bond, A. D. (2005). *Acta Cryst.* C**61**, m356–m358.
Smith, G. (2013). *Acta Cryst.* C**69**, 1472–1477.
Smith, G. & Wermuth, U. D. (2014). *Acta Cryst.* C**70**, 738–741.
Soper, A. K. & Benmore, C. J. (2008). *Phys. Rev. Lett.* **101**, 065502.
Svanberg, L. & Struve, H. (1848). *Phil. Mag. 3rd Ser.* **33**, 409–434.
Toby, B. H. (2001). *J. Appl. Cryst.* **34**, 210–213.
Ullik, F. (1867). *Justus Liebigs Ann. Chem.* **144**, 204–233.
Weil, M. & Bonneau, B. (2014). *Acta Cryst.* E**70**, 54–57.

Westrip, S. P. (2010). *J. Appl. Cryst.* **43**, 920–925.
Zambonini, F. (1923). *Z. Kristallogr*. **58**, 266–292.
Zenker, F. E. (1853). *J. Prakt. Chem*. **58**, 486–492.
Zhilova, S. B., Karov, Z. G. & El'mesova, R. M. (2008). *Russ. J. Inorg. Chem*. **53**, 628–635.

supporting information

Acta Cryst. (2015). E**71**, 799-806 [doi:10.1107/S2056989015011354]

Crystal structures of deuterated sodium molybdate dihydrate and sodium tungstate dihydrate from time-of-flight neutron powder diffraction

A. Dominic Fortes

Computing details

For both compounds, data collection: HRPD control software; cell refinement: *GSAS*/Expgui (Larsen & Von Dreele, 2000: Toby, 2001); data reduction: Mantid (Arnold *et al.*, 2014: Mantid, 2013); program(s) used to solve structure: n/a; program(s) used to refine structure: *GSAS*/Expgui (Larsen & Von Dreele, 2000: Toby, 2001); molecular graphics: *DIAMOND* (Putz & Brandenburg, 2006); software used to prepare material for publication: *publCIF* (Westrip, 2010).

(Na2MoO4.2D2O) Disodium molybdenum(VI) oxide dihydrate

Crystal data

$Na_2MoO_4{\cdot}2D_2O$
M_r = 245.99
Orthorhombic, *Pbca*
Hall symbol: -P 2ac 2ab
a = 8.482961 (14) Å
b = 10.566170 (17) Å
c = 13.83195 (3) Å
V = 1239.79 (1) Å^3
Z = 8
D_x = 2.636 Mg m^{-3}
Melting point: 353 K
Neutron radiation
μ = 0.03+ 0.0007 * λ mm^{-1}
T = 295 K
white
cylinder, 38 × 11 mm
Specimen preparation: Prepared at 323 K and 100 kPa

Data collection

HRPD, High resolution neutron powder diffractometer
Radiation source: ISIS Facility, Neutron spallation source
Specimen mounting: vanadium tube
Data collection mode: transmission
Scan method: time of flight
Absorption correction: analytical
Data were corrected for self shielding using σ_{scatt} = 93.812 barns and $\sigma_{ab}(\lambda)$ = 3.657 barns at 1.798 Å during the normalisation procedure. The linear absorption coefficient is wavelength dependent and is calculated as: μ = 0.0308 + 0.0007 * λ [mm^{-1}]
T_{min} = 0.685, T_{max} = 0.706
$2\theta_{fixed}$ = 168.329
Distance from source to specimen: 95000 mm
Distance from specimen to detector: 965 mm

Refinement

Least-squares matrix: full
$R_p = 0.013$
$R_{wp} = 0.013$
$R_{exp} = 0.007$
$R(F^2) = 0.05255$
$\chi^2 = 3.534$
4610 data points
Excluded region(s): none

Profile function: TOF profile function #3 (21 terms). Profile coefficients for exp pseudovoigt convolution [Von Dreele, 1990 (unpublished)] (α) = 0.1414, (β_0) = 0.026250, (β_1) = 0.004690, (σ_0) = 0, (σ_1) = 194.5, (σ_2) = 13.5, (γ_0) = 0, (γ_1) = 0, (γ_2) = 0, (γ_{2s}) = 0, (γ_{1e}) = 0, (γ_{2e}) = 0, (ε_i) = 0, (ε_a) = 0, (ε_A) = 0, (γ_{11}) = 0.057, (γ_{22}) = 0, (γ_{33}) = 0.059, (γ_{12}) = -0.087, (γ_{13}) = -0.014, (γ_{23}) = -0.018. Peak tails ignored where intensity <0.0010x peak. Aniso. broadening axis 0.0 0.0 1.0
133 parameters
0 restraints
0 constraints
$(\Delta/\sigma)_{max} = 0.03$
Background function: GSAS Background function number 1 with 12 terms. Shifted Chebyshev function of 1st kind 1: 4.30598, 2: 1.54022, 3: -0.237828 4: -6.992080x10^{-2}, 5: -0.113274, 6: -1.736560x10^{-2}, 7: -1.996810x10^{-2}, 8: 2.118030x10^{-5}, 9: -4.698340x10^{-3}, 10: -2.646770x10^{-2}, 11: 2.772870x10^{-2}, 12: -1.690170x10^{-3}

Fractional atomic coordinates and isotropic or equivalent isotropic displacement parameters (Å²)

	x	*y*	*z*	U_{iso}*/U_{eq}
Mo1	0.51477 (10)	0.80193 (8)	0.52313 (8)	0.01137
Na1	0.3438 (3)	0.4964 (2)	0.58515 (17)	0.02371
Na2	0.7433 (2)	0.5509 (2)	0.64802 (16)	0.0216
O1	0.45103 (15)	0.82353 (12)	0.40216 (9)	0.01917
O2	0.55667 (15)	0.64011 (10)	0.54111 (10)	0.01665
O3	0.68676 (15)	0.89087 (11)	0.53936 (11)	0.02282
O4	0.37187 (15)	0.85121 (12)	0.60907 (10)	0.0194
O5	0.53793 (19)	0.40846 (16)	0.70077 (14)	0.0252
O6	0.2281 (2)	0.64176 (17)	0.70081 (11)	0.02505
D51	0.5576 (2)	0.32908 (18)	0.66668 (13)	0.03656
D52	0.5585 (2)	0.39149 (15)	0.76825 (14)	0.03068
D61	0.1235 (2)	0.64696 (14)	0.67235 (12)	0.03034
D62	0.27890 (19)	0.71840 (16)	0.67765 (12)	0.03232

Atomic displacement parameters (Å²)

	U^{11}	U^{22}	U^{33}	U^{12}	U^{13}	U^{23}
Mo1	0.0103 (6)	0.0083 (5)	0.0156 (6)	0.0001 (4)	0.0009 (5)	0.0003 (5)
Na1	0.0249 (13)	0.0213 (11)	0.0250 (15)	−0.0011 (10)	0.0026 (10)	0.0012 (9)
Na2	0.0196 (12)	0.0180 (12)	0.0272 (14)	−0.0037 (9)	0.0008 (9)	−0.0006 (10)
O1	0.0188 (7)	0.0191 (7)	0.0196 (8)	0.0025 (6)	0.0004 (6)	0.0017 (6)
O2	0.0161 (6)	0.0086 (6)	0.0252 (8)	−0.0008 (6)	−0.0019 (6)	0.0017 (6)
O3	0.0197 (7)	0.0199 (7)	0.0289 (9)	−0.0079 (6)	−0.0020 (6)	−0.0022 (7)

O4	0.0187 (6)	0.0163 (6)	0.0233 (8)	0.0040 (6)	0.0050 (6)	−0.0011 (6)
O5	0.0272 (9)	0.0207 (9)	0.0277 (10)	−0.0006 (7)	−0.0036 (8)	0.0001 (8)
O6	0.0264 (9)	0.0257 (9)	0.0231 (10)	−0.0018 (8)	−0.0031 (7)	0.0060 (7)
D51	0.0432 (11)	0.0272 (9)	0.0393 (11)	0.0030 (8)	−0.0107 (9)	−0.0006 (9)
D52	0.0399 (9)	0.0292 (8)	0.0229 (8)	0.0008 (8)	−0.0003 (8)	0.0027 (8)
D61	0.0233 (9)	0.0340 (9)	0.0337 (9)	0.0004 (7)	−0.0062 (8)	0.0030 (8)
D62	0.0338 (10)	0.0248 (8)	0.0384 (12)	−0.0056 (8)	−0.0024 (8)	0.0028 (8)

Geometric parameters (Å, º)

Mo1—O1	1.7732 (17)	Na2—O3^{v}	2.339 (3)
Mo1—O2	1.7640 (14)	Na2—O5	2.415 (3)
Mo1—O3	1.7499 (16)	Na2—O6^{vi}	2.305 (3)
Mo1—O4	1.7759 (17)	O5—D51	0.9766 (19)
Na1—O2	2.437 (3)	O5—D52	0.9664 (18)
Na1—O2^{i}	2.417 (3)	O6—D61	0.9722 (16)
Na1—O3^{ii}	2.482 (3)	O6—D62	0.9719 (18)
Na1—O4^{iii}	2.410 (3)	D51—O1^{i}	1.874 (2)
Na1—O5	2.476 (2)	D52—O4^{vii}	1.846 (3)
Na1—O6	2.426 (3)	D61—O1^{ii}	1.816 (2)
Na2—O1^{iv}	2.312 (3)	D62—O4	1.868 (3)
Na2—O2	2.363 (3)		

O1—Mo1—O2	108.62 (8)	O2^{i}—Na1—O6	174.75 (13)
O1—Mo1—O3	107.83 (8)	O4^{iii}—Na1—O5	100.22 (10)
O1—Mo1—O4	112.69 (8)	O4^{iii}—Na1—O6	90.30 (9)
O2—Mo1—O3	109.54 (7)	O5—Na1—O6	94.63 (10)
O2—Mo1—O4	109.11 (8)	O1^{iv}—Na2—O2	95.39 (9)
O3—Mo1—O4	109.01 (8)	O1^{iv}—Na2—O3^{v}	91.65 (9)
O2—Na1—O2^{i}	86.12 (8)	O1^{iv}—Na2—O5	176.34 (12)
O2—Na1—O3^{ii}	85.70 (9)	O1^{iv}—Na2—O6^{vi}	94.37 (9)
O2—Na1—O4^{iii}	173.42 (12)	O2—Na2—O3^{v}	93.22 (9)
O2—Na1—O5	84.40 (9)	O2—Na2—O5	87.38 (8)
O2—Na1—O6	94.02 (10)	O2—Na2—O6^{vi}	111.35 (10)
O3^{ii}—Na1—O2^{i}	88.43 (9)	O3^{v}—Na2—O5	85.79 (9)
O3^{ii}—Na1—O4^{iii}	89.62 (9)	O3^{v}—Na2—O6^{vi}	153.97 (12)
O3^{ii}—Na1—O5	170.10 (11)	O5—Na2—O6^{vi}	86.84 (10)
O3^{ii}—Na1—O6	86.35 (9)	D51—O5—D52	106.0 (2)
O2^{i}—Na1—O4^{iii}	89.13 (9)	D61—O6—D62	103.0 (2)
O2^{i}—Na1—O5	90.61 (10)		

Symmetry codes: (i) −*x*+1, −*y*+1, −*z*+1; (ii) *x*−1/2, −*y*+3/2, −*z*+1; (iii) −*x*+1/2, *y*−1/2, *z*; (iv) *x*+1/2, −*y*+3/2, −*z*+1; (v) −*x*+3/2, *y*−1/2, *z*; (vi) *x*+1/2, *y*, −*z*+3/2; (vii) −*x*+1, *y*−1/2, −*z*+3/2.

(Na2WO4.2D2O) Disodium tungsten(VI) oxide dihydrate

Crystal data

$Na_2WO_4·2D_2O$
M_r = 333.87

Orthorhombic, *Pbca*
Hall symbol: -P 2ac 2ab

a = 8.482514 (15) Å
b = 10.595156 (19) Å
c = 13.85640 (3) Å
V = 1245.32 (1) Å^3
Z = 8
D_x = 3.562 Mg m^{-3}
Melting point: 373 K

Data collection

HRPD, High resolution neutron powder diffractometer
Radiation source: ISIS Facility, Neutron spallation source
Specimen mounting: vanadium tube
Data collection mode: transmission
Scan method: time of flight

Neutron radiation
μ = 0.03+ 0.0033 * λ mm^{-1}
T = 295 K
white
cylinder, 50 × 11 mm
Specimen preparation: Prepared at 323 K and 100 kPa

Absorption correction: analytical
Data were corrected for self shielding using σ_{scatt} = 94.190 barns and $\sigma_{ab}(\lambda)$ = 19.484 barns at 1.798 Å during the normalisation procedure. The linear absorption coefficient is wavelength dependent and is calculated as: μ = 0.0284 + 0.0033 * λ [mm^{-1}]
T_{min} = 0.603, T_{max} = 0.700
$2\theta_{fixed}$ = 168.329
Distance from source to specimen: 95000 mm
Distance from specimen to detector: 965 mm

Refinement

Least-squares matrix: full
R_p = 0.014
R_{wp} = 0.013
R_{exp} = 0.007
$R(F^2)$ = 0.04597
χ^2 = 3.312
4610 data points
Excluded region(s): none

Profile function: TOF profile function #3 (21 terms). Profile coefficients for exp pseudovoigt convolution [Von Dreele, 1990 (unpublished)] (α) = 0.1414, (β_0) = 0.026250, (β_1) = 0.004690, (σ_0) = 0, (σ_1) = 322.9, (σ_2) = 15.7, (γ_0) = 0, (γ_1) = 0, (γ_2) = 0, (γ_{2s}) = 0, (γ_{1e}) = 0, (γ_{2e}) = 0, (ε_i) = 0, (ε_a) = 0, (ε_A) = 0, (γ_{11}) = 0.023, (γ_{22}) = 0, (γ_{33}) = 0.006, (γ_{12}) = 0.050, (γ_{13}) = 0.016, (γ_{23}) = 0.017. Peak tails ignored where intensity <0.0010x peak. Aniso. broadening axis 0.0 0.0 1.0
133 parameters
0 restraints
0 constraints
$(\Delta/\sigma)_{max}$ = 0.04
Background function: GSAS Background function number 1 with 12 terms. Shifted Chebyshev function of 1st kind 1: 3.91163, 2: 1.22805, 3: -0.206144, 4: -8.53351x10^{-2}, 5: -9.966470x10^{-2}, 6: -1.847470x10^{-2}, 7: -1.38195x10^{-2}, 8: 9.956170x10^{-4}, 9: 4.49839x10^{-3}, 10: -2.199010x10^{-2}, 11: 2.57524x10^{-2}, 12: -2.00574x10^{-3}

Fractional atomic coordinates and isotropic or equivalent isotropic displacement parameters (Å^2)

	x	y	z	U_{iso}*/U_{eq}
W1	0.51352 (13)	0.80186 (10)	0.52310 (10)	0.01206
Na1	0.3444 (2)	0.4957 (2)	0.58501 (16)	0.02213
Na2	0.7422 (2)	0.54966 (18)	0.64745 (14)	0.02166
O1	0.44940 (14)	0.82253 (11)	0.40144 (8)	0.01858
O2	0.55647 (14)	0.63936 (9)	0.54135 (9)	0.01675
O3	0.68666 (14)	0.89213 (10)	0.53870 (10)	0.02256

O4	0.36916 (14)	0.85058 (11)	0.60895 (9)	0.01972
O5	0.53794 (17)	0.40814 (14)	0.70116 (12)	0.02505
O6	0.2276 (2)	0.64134 (14)	0.70148 (11)	0.02531
D51	0.5576 (2)	0.32926 (17)	0.66767 (12)	0.03829
D52	0.55912 (18)	0.39189 (14)	0.76800 (13)	0.03325
D61	0.1229 (2)	0.64645 (13)	0.67384 (10)	0.03267
D62	0.27774 (17)	0.71764 (15)	0.67874 (12)	0.03524

Atomic displacement parameters (Å²)

	U^{11}	U^{22}	U^{33}	U^{12}	U^{13}	U^{23}
W1	0.0099 (7)	0.0064 (6)	0.0199 (7)	−0.0002 (5)	0.0009 (6)	0.0002 (6)
Na1	0.0209 (11)	0.0167 (9)	0.0289 (13	0.0004 (9)	0.0028 (9)	0.0003 (8)
Na2	0.0192 (10)	0.0183 (11)	0.0275 (13)	0.0001 (8)	−0.0006 (8)	0.0000 (9)
O1	0.0170 (6)	0.0192 (6)	0.0195 (7)	0.0008 (5)	0.0010 (6)	0.0031 (5)
O2	0.0176 (6)	0.0079 (5)	0.0248 (7)	0.0014 (5)	−0.0004 (5)	0.0035 (5)
O3	0.0193 (7)	0.0190 (6)	0.0293 (8)	−0.0083 (5)	−0.0002 (6)	−0.0015 (6)
O4	0.0201 (6)	0.0176 (6)	0.0214 (7)	0.0045 (5)	0.0052 (6)	0.0008 (6)
O5	0.0305 (9)	0.0206 (9)	0.0241 (8)	−0.0027 (7)	−0.0031 (7)	−0.0023 (7)
O6	0.0246 (8)	0.0247 (8)	0.0266 (9)	−0.0004 (7)	−0.0046 (7)	0.0061 (7)
D51	0.0448 (10)	0.0304 (9)	0.0397 (9)	−0.0001 (8)	−0.0104 (8)	−0.0032 (8)
D52	0.0415 (9)	0.0323 (8)	0.0259 (8)	−0.0027 (7)	−0.0001 (8)	0.0004 (7)
D61	0.0259 (9)	0.0354 (9)	0.0367 (9)	−0.0011 (7)	−0.0030 (7)	0.0046 (8)
D62	0.0347 (9)	0.0270 (8)	0.0440 (11)	−0.0059 (7)	−0.0029 (7)	0.0059 (7)

Geometric parameters (Å, º)

W1—O1	1.7849 (19)	Na2—O3^{v}	2.328 (2)
W1—O2	1.7779 (15)	Na2—O5	2.409 (3)
W1—O3	1.7659 (17)	Na2—O6^{vi}	2.311 (2)
W1—O4	1.7834 (18)	O5—D51	0.9702 (18)
Na1—O2	2.433 (2)	O5—D52	0.9591 (16)
Na1—O2^{i}	2.412 (3)	O6—D61	0.9684 (16)
Na1—O3^{ii}	2.479 (3)	O6—D62	0.9664 (16)
Na1—O4^{iii}	2.399 (2)	D51—O1^{i}	1.873 (2)
Na1—O5	2.479 (3)	D52—O4^{vii}	1.863 (2)
Na1—O6	2.443 (3)	D61—O1^{ii}	1.834 (2)
Na2—O1^{iv}	2.320 (2)	D62—O4	1.876 (2)
Na2—O2	2.355 (2)		

O1—W1—O2	108.40 (9)	O2^{i}—Na1—O6	174.55 (12)
O1—W1—O3	107.61 (8)	O4^{iii}—Na1—O5	99.82 (9)
O1—W1—O4	112.66 (8)	O4^{iii}—Na1—O6	90.40 (8)
O2—W1—O3	109.67 (7)	O5—Na1—O6	94.37 (10)
O2—W1—O4	109.03 (9)	O1^{iv}—Na2—O2	95.10 (8)
O3—W1—O4	109.43 (9)	O1^{iv}—Na2—O3^{v}	91.90 (8)
O2—Na1—O2^{i}	86.16 (7)	O1^{iv}—Na2—O5	176.73 (11)
O2—Na1—O3^{ii}	85.82 (8)	O1^{iv}—Na2—O6^{vi}	93.43 (9)

O2—Na1—O4^{iii}	173.55 (11)	O2—Na2—O3^{v}	93.36 (8)
O2—Na1—O5	84.60 (8)	O2—Na2—O5	87.87 (7)
O2—Na1—O6	93.95 (9)	O2—Na2—O6^{vi}	111.09 (9)
O3^{ii}—Na1—O2^{i}	88.32 (8)	O3^{v}—Na2—O5	86.57 (8)
O3^{ii}—Na1—O4^{iii}	89.72 (8)	O3^{v}—Na2—O6^{vi}	154.35 (11)
O3^{ii}—Na1—O5	170.42 (10)	O5—Na2—O6^{vi}	86.74 (9)
O3^{ii}—Na1—O6	86.26 (8)	D51—O5—D52	105.96 (19)
O2^{i}—Na1—O4^{iii}	89.05 (8)	D61—O6—D62	103.18 (19)
O2^{i}—Na1—O5	91.07 (9)		

Symmetry codes: (i) −*x*+1, −*y*+1, −*z*+1; (ii) *x*−1/2, −*y*+3/2, −*z*+1; (iii) −*x*+1/2, *y*−1/2, *z*; (iv) *x*+1/2, −*y*+3/2, −*z*+1; (v) −*x*+3/2, *y*−1/2, *z*; (vi) *x*+1/2, *y*, −*z*+3/2; (vii) −*x*+1, *y*−1/2, −*z*+3/2.